

Electronic Supplementary Information

Autonomous Self-Healing Supramolecular Elastomer Reinforced and Toughened by Graphitic Carbon Nitride Nanosheets Tailored for Smart Anticorrosion Coating Applications

JianHua Xu,^a Sheng Ye,^a ChenDi Ding,^a LingHua Tan,^b and JiaJun Fu^{*a}

^aSchool of Chemical Engineering, Nanjing University of Science and Technology, Nanjing, 210094, People's Republic of China

^bNational Special Superfine Power Engineering Research Center, Nanjing University of Science and Technology, Nanjing, 210094, People's Republic of China

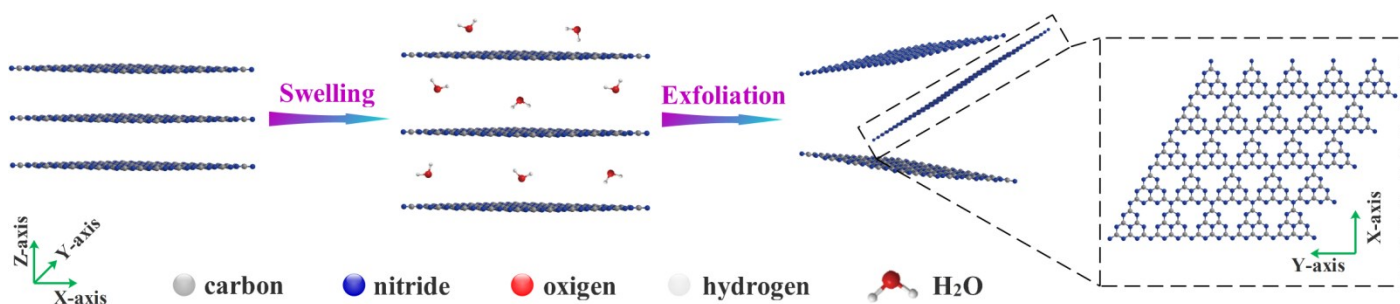
E-mail:

fujiajun668@gmail.com

Table of Contents

1.	Supplementary
Figures.....	3
2.	Supplementary
Tables.....	12
3. Supplementary Movie.....	13
Reference.....	14

1. Supplementary Figures



Scheme S1 Schematic illustration of liquid-exfoliation process from bulk $g\text{-C}_3\text{N}_4$ to ultrathin nanosheets.

The surface energy of water is matching of bulk $g\text{-C}_3\text{N}_4$. Thus, as shown in scheme S1, bulk $g\text{-C}_3\text{N}_4$ materials can be swelled and the exfoliated into ultrathin $g\text{-C}_3\text{N}_4$ nanosheets by liquid-exfoliation process using water as solvent.

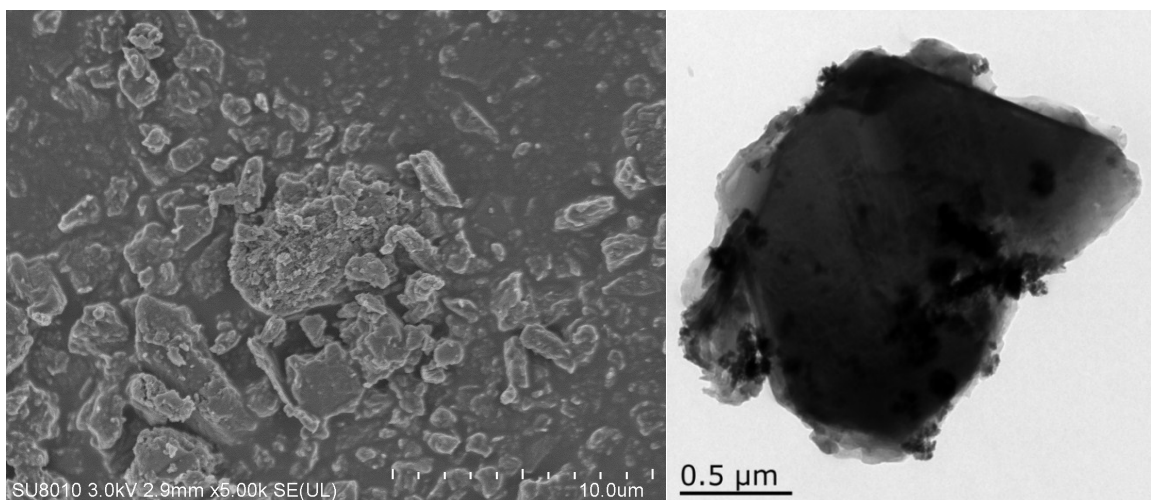


Fig.S1 SEM and TEM images of bulk $g\text{-C}_3\text{N}_4$.

SEM and TEM images indicate that bulk $g\text{-C}_3\text{N}_4$ display a laminated structure, which is similar to its analogue graphite, containing many stacking layers. Furthermore, compared with exfoliated $g\text{-C}_3\text{N}_4$ NSs (Fig. 2a), the size and thickness of bulk $g\text{-C}_3\text{N}_4$ are much larger.

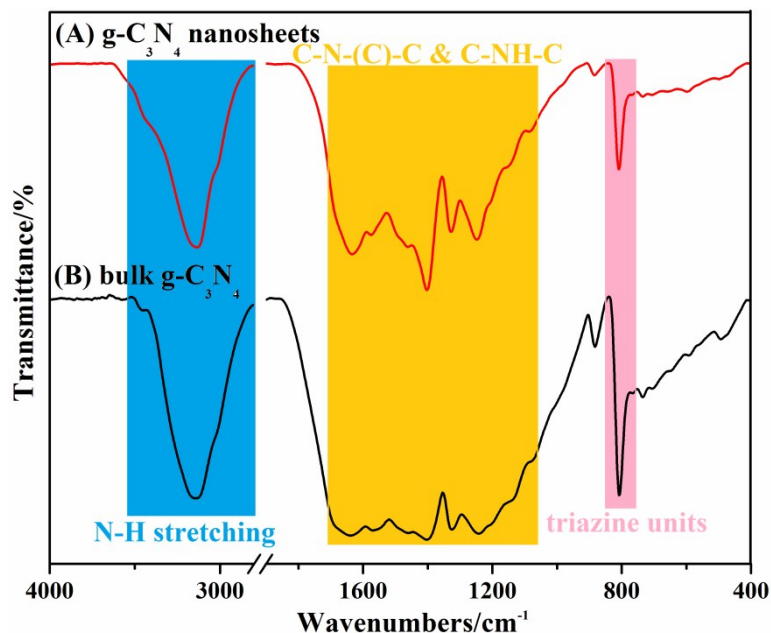


Fig.S2 FT-IR spectra of bulk $g\text{-C}_3\text{N}_4$ and $g\text{-C}_3\text{N}_4$ NSs.

The FT-IR spectrum of $g\text{-C}_3\text{N}_4$ NSs is almost identical with the bulk $g\text{-C}_3\text{N}_4$, indicating that no extra functional groups are formed during the exfoliation process. Specifically, the peak at 807 cm^{-1} is assigned to the out-of-plane skeletal bending modes of the C-N heterocycles. Meanwhile, several bands located in $1000\text{-}1800\text{ cm}^{-1}$ are ascribed to the stretching vibration of the connected units of C-N(-C)-C or C-NH-C. Besides, the bands in the range of $3000\text{-}3600\text{ cm}^{-1}$ give strong evidence of the N-H stretching vibration, which are regarded as the interfacial hydrogen-bonding motifs.

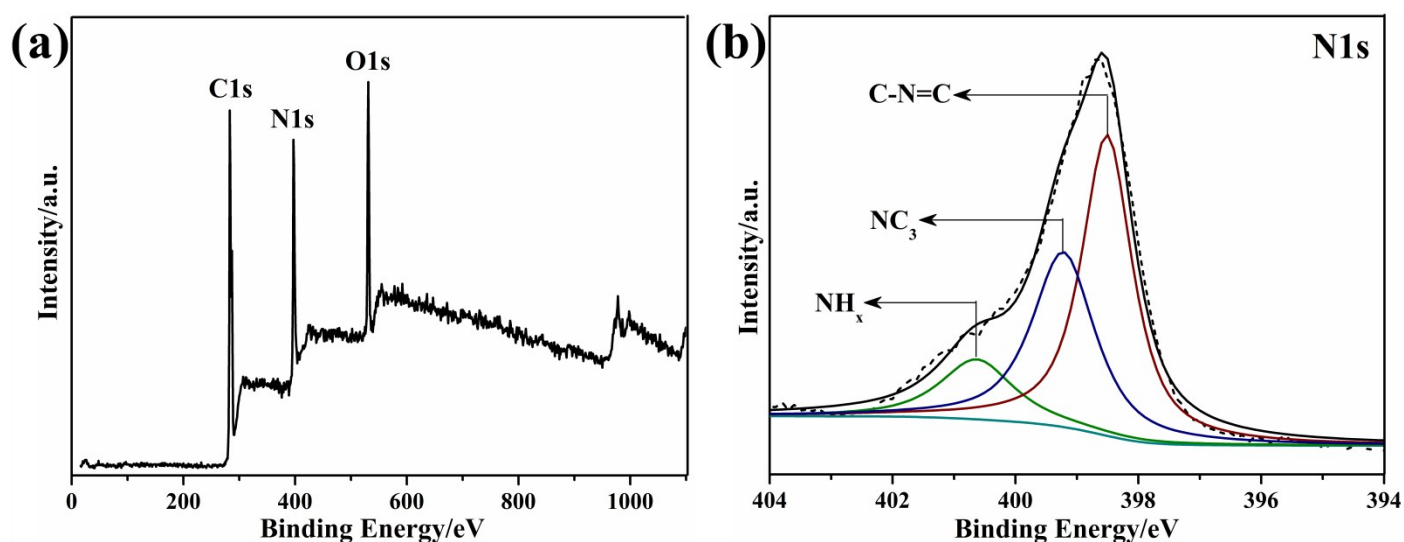


Fig. S3 XPS spectra of $g\text{-C}_3\text{N}_4$ NSs: (a) full scan, (b) high resolution N1s.

The high-resolution N1s spectrum of $g\text{-C}_3\text{N}_4$ NSs can be deconvoluted into three types of N-related bonding (Fig.S3b). In detail, the peaks located at 398.5 , 399.2 and 400.6 eV are assigned to the pyridine nitrogen in triazine rings (C-N=C), tertiary nitrogen N(-C)₃ groups and amino functional groups (NH_x), respectively. In accordance with the FT-IR results, XPS analysis also demonstrate that $g\text{-C}_3\text{N}_4$ NSs possess many intrinsic functional groups, such as $-\text{NH}_2$ or $-\text{NH}$, which can be used as reactive sites or interfacial hydrogen-bonding motifs.¹

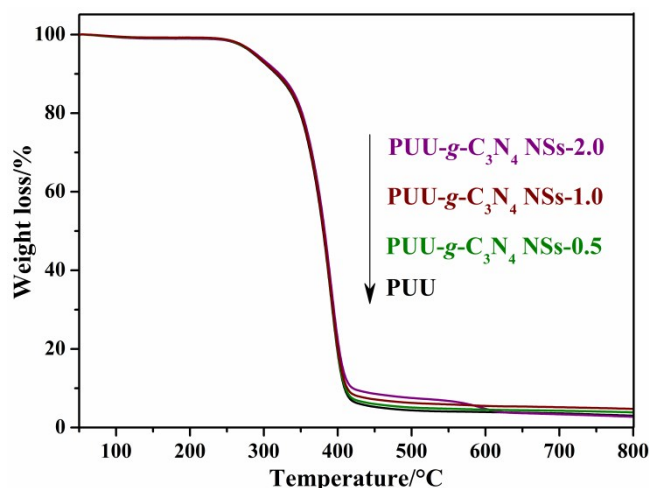


Fig.S4 TGA curves of PUU- g -C₃N₄ NSs-x materials.

As can be seen in Fig. S4, two stages are visible in the thermal weight loss process of PUU- g -C₃N₄ NSs-x polymer. The first stage beginning at 100 °C is assigned to the traces of moisture, whereas the second stage beginning at about 250 °C is corresponding to initial decomposition process of PUU matrix. Significantly, the thermal stability of PUU is not influenced by the introduction of g -C₃N₄NSs (initial decomposition temperature is still at 250 °C). The TGA curves demonstrate that PUU- g -C₃N₄-x(x=0-2.0) materials exhibit excellent thermal stability.

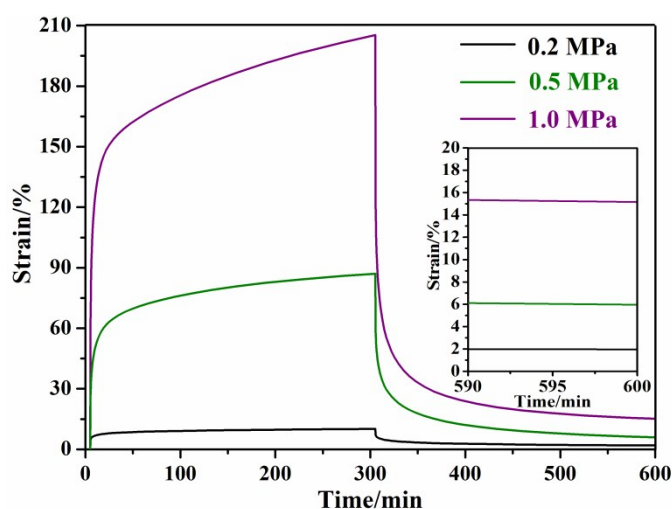


Fig. S5 Creep recovery experiments performed on PUU- g -C₃N₄ NSs-1.0 material at varying stress.

Creep recovery experiments confirm that the hydrogen bonded network can sustain significant load. As shown in Fig.S5, a stress of 0.2 MPa was applied of 300 min, which led to an instantaneous strain of 6% that increases at a rate of about 0.4% per hour in the steady-state creep region. Upon releasing the applied stress, the sample almost completely recovered to its original dimensions with negligible residual strain (\approx 2%). For comparison, a medium stress of 0.5 MPa applied for the same time resulted in an instantaneous strain of 40% that increased at a rate of about 3.4% per hour in the steady-state creep region, releasing the applied stress leaves residual strain of about 5.7%. Besides, applying a high stress of 1MPa under the same conditions led to large strain of \approx 200%, which increases at a rate of about 10.3% per hour in the steady-state creep region. Subsequently, releasing the stress left residual strain of 15%.

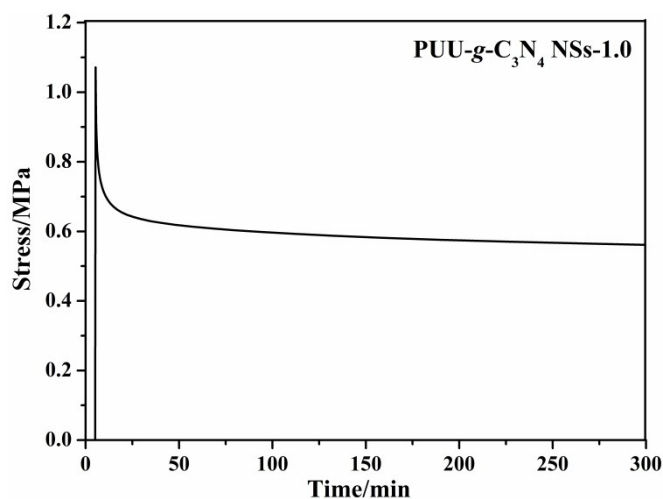


Fig. S6 Stress relaxation experiment performed on PUU- g - C_3N_4 NSs-1.0 material.

The sample were quickly stretched to 100% strain and then set at this strain for relaxation for 300 min (the corresponding instantaneous stress is about 1.1 MPa). Then the applied stress was relaxed rapidly to 0.8 MPa within 5 min. Subsequently, the residual stress was relaxed slowly for a final stress of about 0.55 MPa at 300 min at 100% strain. Both of the creep recovery and stress relaxation experiments demonstrate that multivalent hydrogen bonds existing in polymer network can form a robust polymer network, which can support large load during stretching process.

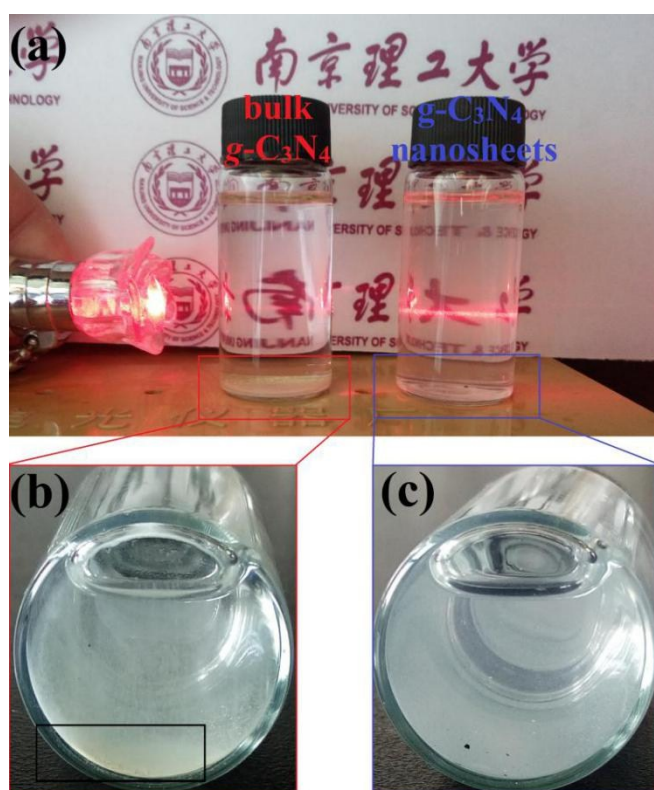


Fig. S7 (a) Comparison of the dispersion of bulk g - C_3N_4 and g - C_3N_4 NSs in DMF solution. (b) and (c) is the magnified images of small bottle in (a), which also prove the dispersion states.

10 mg bulk g - C_3N_4 and g - C_3N_4 NSs dispersed in 10 mL DMF ($1 \text{ mg} \cdot \text{mL}^{-1}$), respectively, and then the as-prepared dispersion liquid samples were placed for 24 h for comparison. As shown in Fig. S7, the g - C_3N_4 NSs solution exhibits well-defined Tyndall effect, whereas the bulk g - C_3N_4 inescapably aggregate in the bottom of bottle from DMF solution.

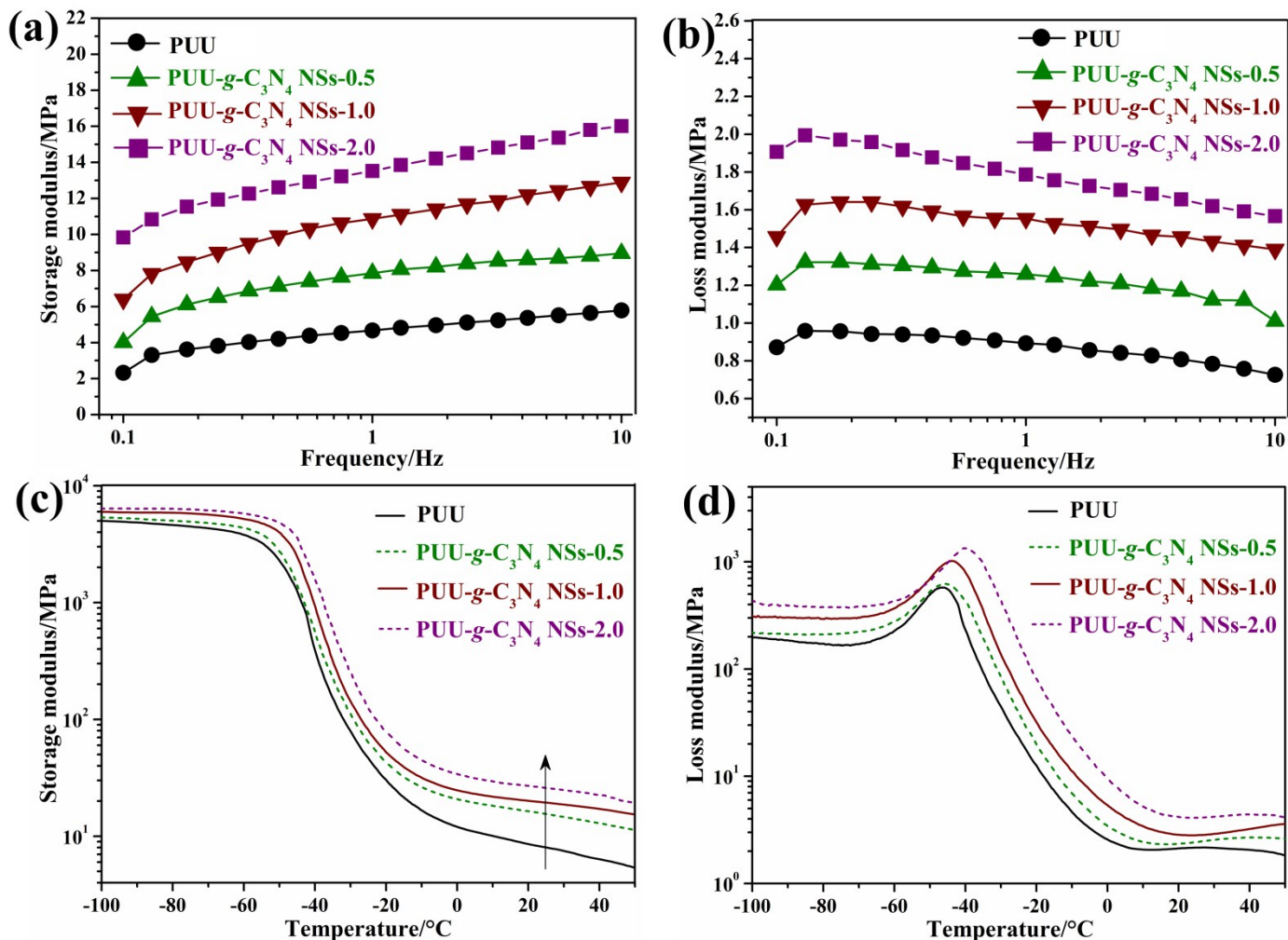


Fig.S8 DMA results: Temperature dependence of the (a) G' and (b) G'' of PUU- g -C₃N₄ NSs- x materials; frequency dependence of the (c) G' and (d) G'' of PUU- g -C₃N₄ NSs- x materials.

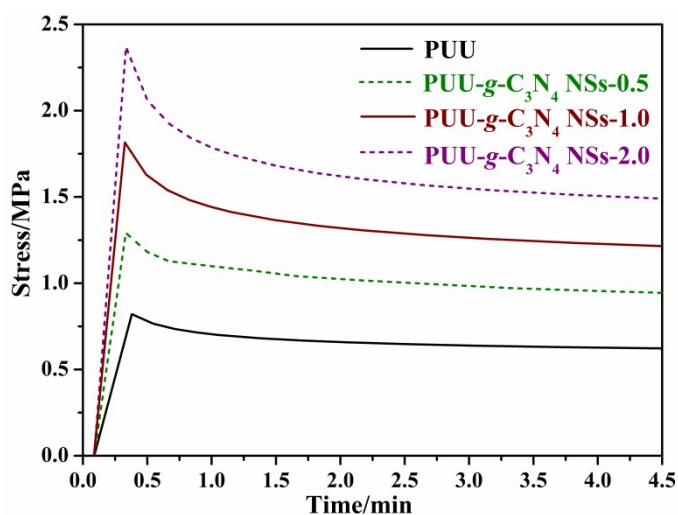


Fig. S9 Stress-relaxation curves of PUU- g -C₃N₄ NSs- x materials at 25 °C. The samples used for the test were stretched to a strain of 100% and held constant for 4 min.

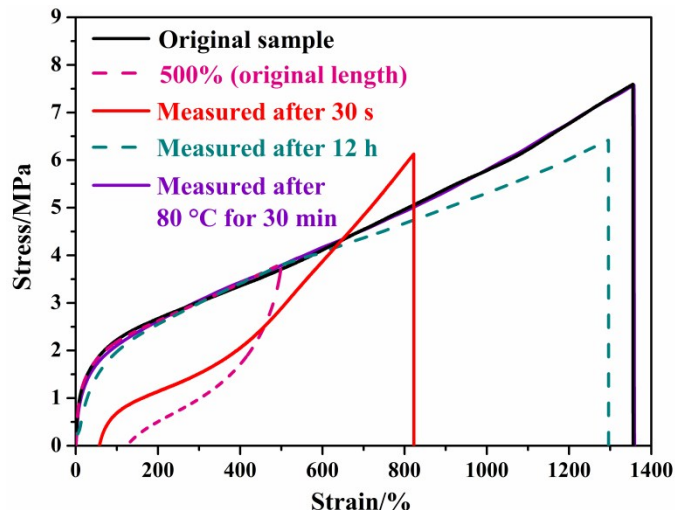


Fig. S10 Tensile test of the PUU-*g*-C₃N₄ NSs-1.0 material upon waiting for 30 s (red curve) after loading and unloading cycle (strain of 500%, pink curve), and the sample which was left to self-recovery for 12 h under room temperature and 30 min at 80 °C, respectively.

As can be seen in Fig. S10, prolonging waiting time from 30 s to 12 h under room temperature, the stress-strain curve of the self-recovery sample gradually approached to the normal sample (black curve). Notably, after heating at 80 °C for 30 min, the loading/unloading curve (purple curve) almost overlapped with the normal run, indicating the complete self-recovery of the polymer network through the reformation of intermolecular/interfacial hydrogen bonds.

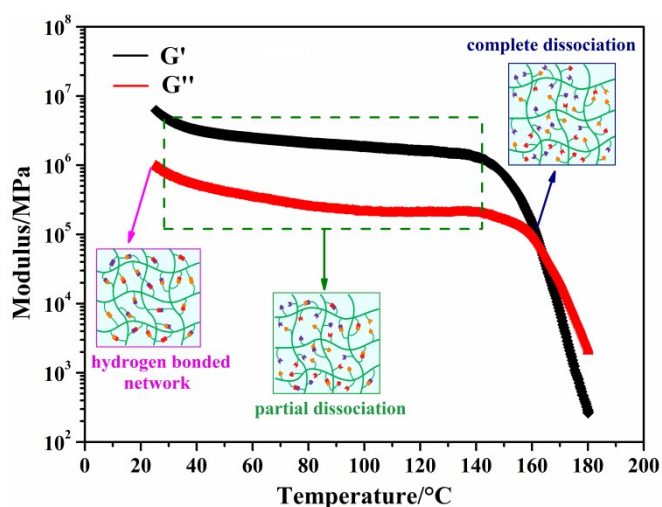


Fig. S11 Temperature-dependent rheological behavior of PUU material by frequency of 1 Hz with 0.5% strain.

Temperature-dependent dynamic rheological analysis was employed to investigate the viscoelastic properties of the PUU material. As shown in Fig. S11, in the low temperature regime, the storage modulus (G') was higher than that of loss modulus (G''), indicating the elastic rubbery character clearly governs the properties. With increasing temperature, the G' as well as the G'' gradually decreased, illustrating the partial dissociation of the hydrogen bonded supramolecular network. However, upon the temperature is beyond 140 °C, the drop of storage modulus accelerates quickly, assigned to complete dissociation of the supramolecular PUU matrix and viscous behavior dominates the properties of PUU. In accordance to the temperature-dependent FT-IR testing, the rheological analysis further demonstrates the existence of dynamic hydrogen bonds within PUU matrix.

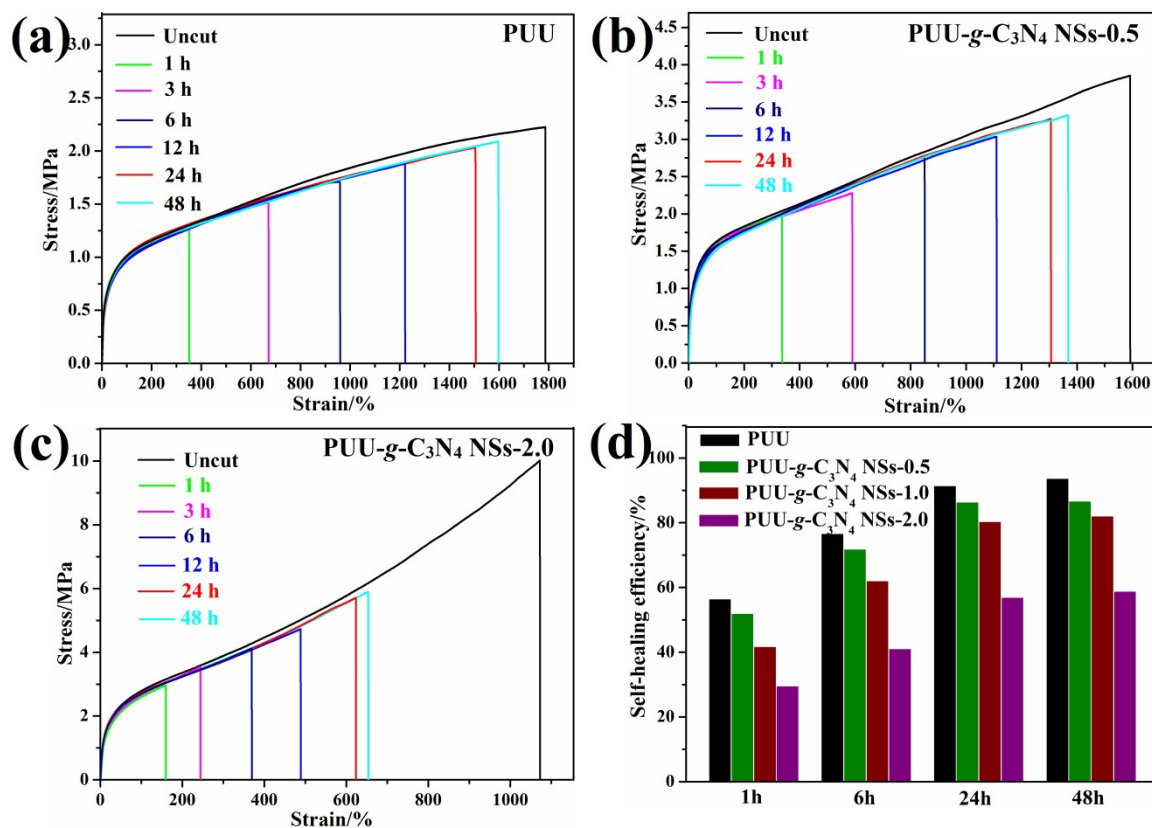


Fig. S12 The stress-strain curves of the self-healing (a) PUU and PUU- g -C₃N₄ NSs- x materials with g -C₃N₄NSs contents at (b) 0.5 wt% and 2.0 wt% at different healing time under room temperature. (d) Comparison of the self-healing efficiencies η of PUU- g -C₃N₄ NSs- x materials at different self-healing time (1, 6, 24 and 48 h).



Fig. S13 The photograph of tensile-failure PUU- g -C₃N₄ NSs-1.0 nanomaterials

When the PUU- g -C₃N₄ NSs-1.0 sample sustains overload, it will undergo irreversible plastic deformation. Meanwhile, large tensile deformation will result in molecular orientation of the polymer. Thus, the tensile-failure PUU- g -C₃N₄ NSs-1.0 material cannot recover to its original length and the size of the fracture surface is very small, which cannot be pushed together for self-healing.

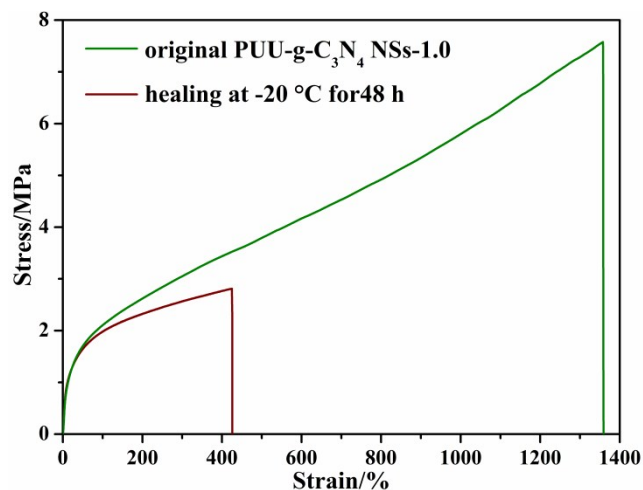


Fig. S14 The stress-strain curves of PUU-*g*-C₃N₄ NSs-1.0 material healed at -20 °C for 48 h.

The healing process even took place at -20 °C to give a recovered tensile stress of 2.84 MPa without any external stimulus (Fig.S14). This value (2.84 MPa) is even higher than many reported elastomers with spontaneous healing ability under room temperature.²⁻⁴

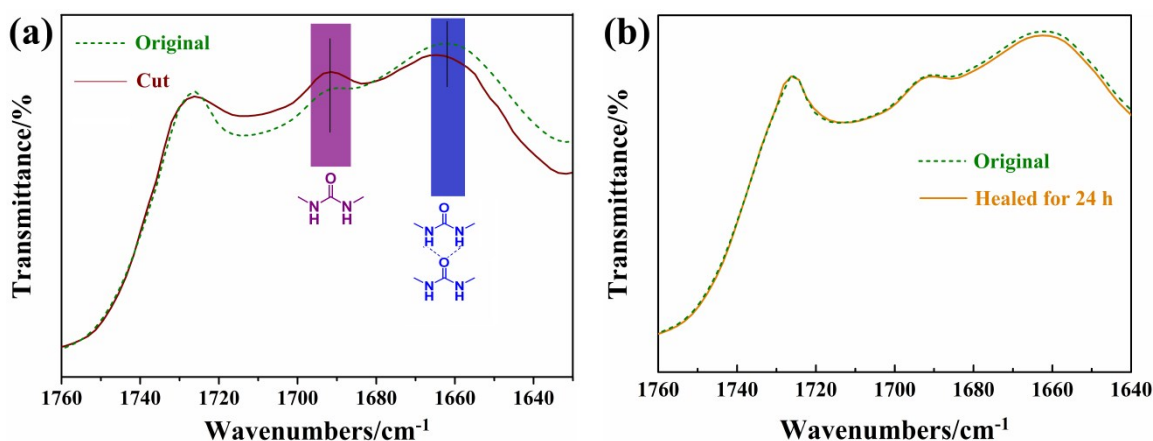


Figure S15. FT-IR spectra collected from (a) undamaged and damaged areas as a function of healing for (b) 0 and (c) 24 h.

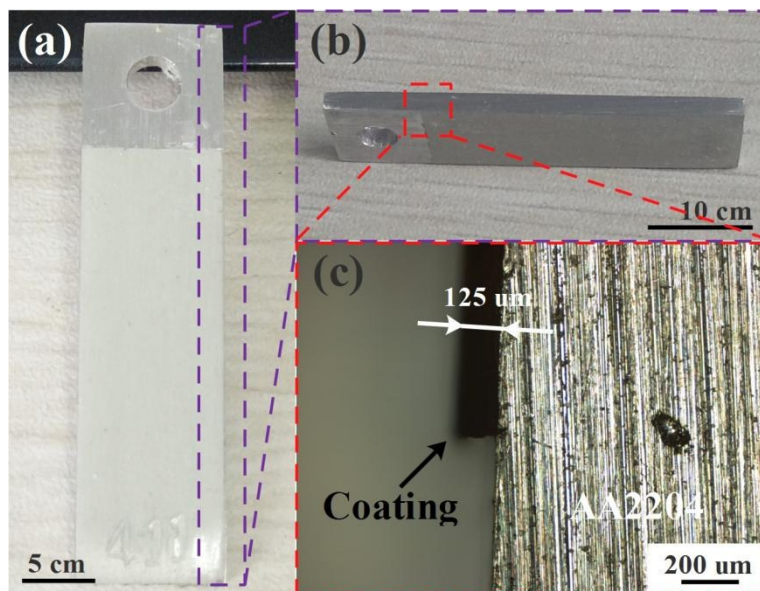


Fig. S16 Photographs of the PUU- g -C₃N₄ NSs anticorrosion coating on AA2024 substrate: (a) frontage and (b) flank; (c) Optical microscopic image for cross-section of PUU- g -C₃N₄ NSs anticorrosion coating.

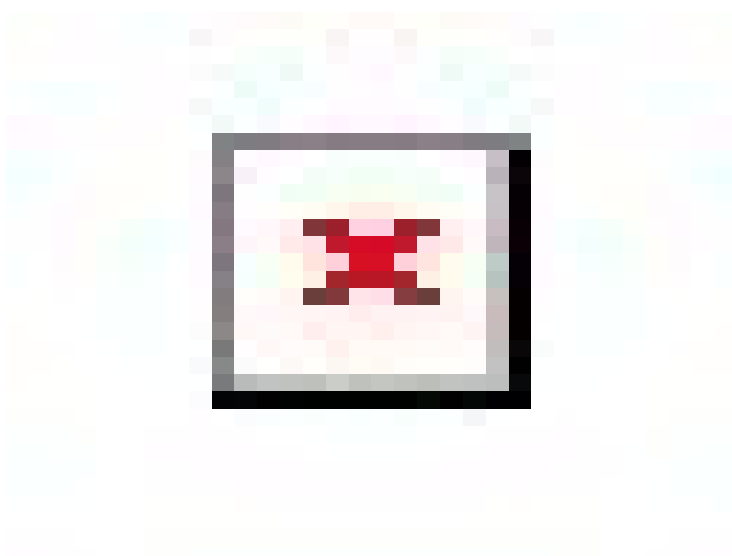


Fig. S17 Comparison of adhesion force of PUU and PUU- g -C₃N₄ NSs ACs.

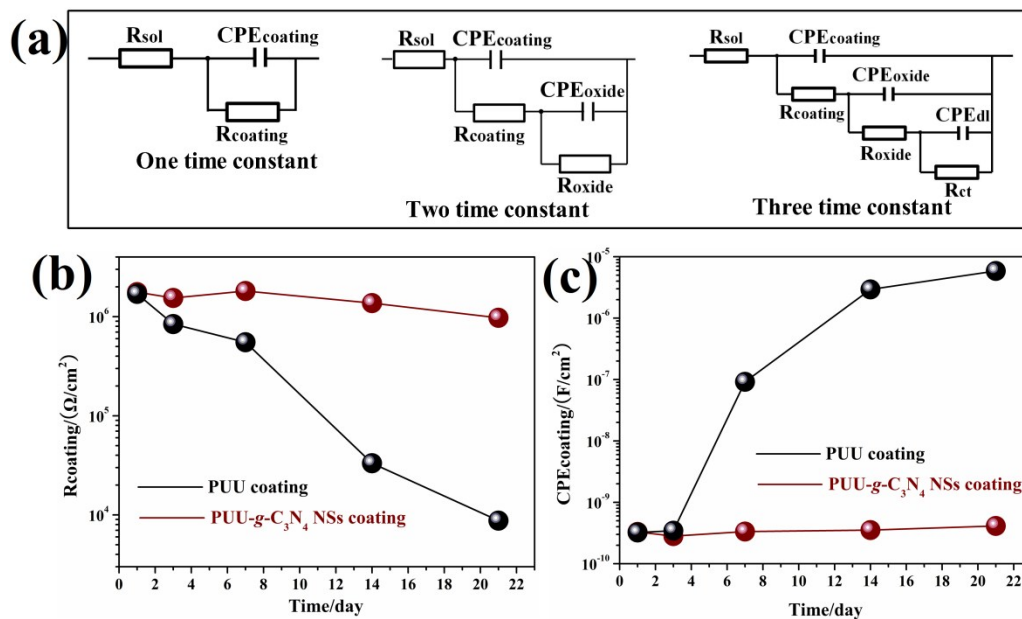


Fig. S18 (a) The equivalent electrical circuits used for bode plots fitting. Evolution of (b) $R_{coating}$ and (c) $CPE_{coating}$ obtained by fitting of bode plots using the appropriate equivalent electrical circuits.

To more accurately explain barrier properties of the tested coatings, the EIS data were fitted using the equivalent electrical circuits (EECs) illustrated in Fig. S15 according to the numbers of time constants. In EECs, R_{sol} , $R_{coating}$, R_{oxide} , and R_{ct} represent the solution resistance, barrier coating (PUU or PUU- $g-C_3N_4$ anticorrosion coating) resistance, aluminum oxide layer resistance and charge transfer resistance, respectively. Constant phase angle (CPE) instead of capacitance is used to obtain the good fit. $CPE_{coating}$, CPE_{oxide} , and CPE_{dl} represent the constant phase element of barrier coating capacitance, aluminum oxide capacitance and double layer capacitance, respectively. As can be seen in Fig. S15 (b) and (c), a dramatic decrease in $R_{coating}$ values and a sharp increase in $CPE_{coating}$ values for PUU anticorrosion coating indicated that PUU anticorrosion coating gradually lost barrier effect due to the water swelling within the coating. By comparison, PUU- $g-C_3N_4$ NSs anticorrosion coating demonstrates the relative stable $R_{coating}$ and $CPE_{coating}$ values during the whole immersion test, suggesting its excellent anti-penetration ability.

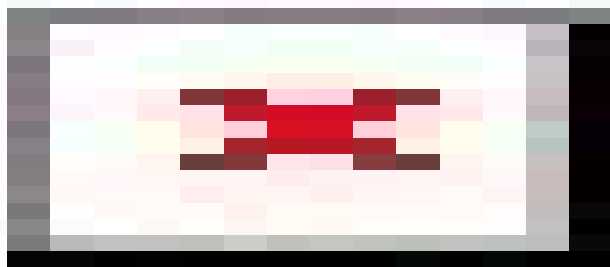


Fig. S19 Tafel curves for PUU and PUU-*g*-C₃N₄ NSs ACs immersing in 3.5 wt% NaCl solution for (a) 30 min and (b) 5 days.

In general, as the more negative corrosion potential and the larger corrosion current density usually correspond to faster corrosion rates while the more positive corrosion potential and the smaller corrosion current density mean a slower corrosion process, thus it can be inferred that PUU-*g*-C₃N₄ NSs AC ($E_{\text{corr}}=-0.68\text{V}$, $I_{\text{corr}}=3.61\times 10^{-11}\text{ A cm}^{-2}$) is significantly less susceptible to corrosion than PUU AC ($E_{\text{corr}}=-0.86\text{V}$, $I_{\text{corr}}=7.24\times 10^{-9}\text{ A cm}^{-2}$). Furthermore, after 5 day immersion, the corrosion current density for PUU-*g*-C₃N₄ AC had a little decrease (from $3.61\times 10^{-11}\text{ A cm}^{-2}$ to $5.44\times 10^{-10}\text{ A cm}^{-2}$), indicating its long-lasting anticorrosion of PUU-*g*-C₃N₄ NSs AC. In comparison, the corrosion current density for PUU AC dramatically decreased from $7.24\times 10^{-9}\text{ A cm}^{-2}$ to $1.05\times 10^{-6}\text{ A cm}^{-2}$, meaning the partial regression of protective ability.

2. Supplementary Table

Table S1 Comparison of the mechanical values of the PUU-bulk g -C₃N₄-2.0 and PUU- g -C₃N₄ NSs-2.0

Fillers	Young's modulus (MPa)	Breaking strength (MPa)	Toughness (MJ/m ³)	Stretch at break (%)
Bulk g -C ₃ N ₄	13.70±0.27	5.48±0.41	35.25±1.32	953±21
g -C ₃ N ₄ NSs	19.53±0.75	10.02±0.72	59.88±1.77	1070±33

Table S2 Comparison of the toughness of the PUU- g -C₃N₄ NSs composite with others

Sample	Fillers	Content wt%	Interfacial force	Toughness MJ·m ³	Amplification %
Polyisoprene/Carbon nanodots ⁵ p(HEMA-co-UPyMA)/OxMWCNT	CDs	≈ 1.0 wt%	Hydrogen bonds	53.7	79%
-α-UPV ⁶	MWCNT	1.0 wt%	Hydrogen bonds	5.63±0.40	0.9 %
Our work	g -C ₃ N ₄ NSs	1.0 wt%	Hydrogen bonds	61.99±1.64	105.2 %

Table S3 Summary of the mechanical and self-healing properties for PUU- g -C₃N₄ NSs-x materials*

Self-healing for 24 h at room temperature

sample	Young's modulus ^a (MPa)	Tensile strength (MPa)	Stretch at break (%)	Toughness ^b (MJ/m ³)	Self-healing efficiency ^c (%)
PUU	7.46±0.44	2.04±0.11	1503±42	23.49±1.03	91.5
PUU- g -C ₃ N ₄ NSs-0.5	12.31±0.25	3.28±0.23	1306±33	31.47±1.31	86.4
PUU- g -C ₃ N ₄ NSs1.0	13.08±0.29	6.10±0.44	1114±25	43.01±1.47	80.4
PUU- g -C ₃ N ₄ NSs-2.0	19.01±0.65	5.71±0.57	623±37	23.81±1.98	57.0

*Strain rate = 100 mm·min⁻¹, 25 °C. ^aYoung's modulus is calculated from the initial slope of stress-strain curves.

^bToughness is calculated by manually integrating the area under the stress-strain curve. ^cSelf-healing efficiency is calculated from the ratio of tensile strength of healed samples to that virgin sample.

3. Supplementary Movie

The file contains supplementary Movie 1 which demonstrates the self-healing capability of PUU-*g*-C₃N₄ NSs-1.0 material. In general, a sample (according to ISO 37-3) was cut into two completely separate pieces with a razor blade. Then, the cut faces were gently pushed together for one minute and the repaired film is left under room temperature for 24 h. Subsequently, the self-healed sample was subject to tensile-stress test under room temperature at a strain rate of 100 mm min⁻¹.

Reference

1. Y. Shi, S. Jiang, K. Zhou, C. Bao, B. Yu, X. Qian, B. Wang, N. Hong, P. Wen and Z. Gui, *ACS Appl. Mater. Inter.*, 2013, **6**, 429-437.
2. J. F. Mei, X. Y. Jia, J. C. Lai, Y. Sun, C. H. Li, J. H. Wu, Y. Cao, X. Z. You and Z. Bao, *Macromol. Rapid Comm.*, 2016, **37**, 1667-1675.
3. K. Guo, D. L. Zhang, X. M. Zhang, J. Zhang, L. S. Ding, B. J. Li and S. Zhang, *Angew. Chem.*, 2015, **127**, 12295-12301.
4. A. Rekondo, R. Martin, A. R. de Luzuriaga, G. Cabañero, H. J. Grande and I. Odriozola, *Mater.Horiz.*, 2014, **1**, 237-240.
5. G. R. Gao, G. L. Du, Y. N. Sun and J. Fu, *ACS Appl. Mater. Interfaces*, 2015, **7**, 5029–5037.
6. T. T. T. Myllymaki, L. Lemetti, Nonoppa and O. Ikkala, *ACS Macro Lett.*, 2017, **6**, 210–214.